Chapter 12
Seismic Detections of Small-Scale Heterogeneities in the Deep Earth

Sebastian Rost, Paul S. Earle, Peter M. Shearer, Daniel A. Frost and Neil D. Selby

Abstract We report the detection of coherent scattered energy related to the phase PKPPKP ($P'P'$) in the data of medium aperture arrays. The scattered energy ($P'\bullet P'$) is weak and requires array processing techniques to extract the signal from the noise. The arrival time window of $P'\bullet P'$ is mostly free from other interfering body wave energy and can be detected over a large distance range. $P'\bullet P'$ has been detected in the data of large aperture arrays previously, but the detection in the data of smaller arrays shows its potential for the study of the small-scale structure of the Earth. Here, we show that $P'\bullet P'$ can detect scattering off small-scale heterogeneities throughout the Earth's mantle from crust to core making this one of the most versatile scattering probes available. We compare the results of $P'\bullet P'$ to a related scattering probe ($PK\bullet KP$). The detected energy is in agreement with stronger scattering, i.e., more heterogeneous structure, in the upper mantle and in an approximately 800-km-thick layer above the core–mantle boundary. Lateral variations in heterogeneity structure can also be detected through differences in scattered energy amplitude. We use an application of the F-statistic in the array processing allowing us a precise measurement of the incidence angles (slowness and backazimuth) of the scattered energy. The directivity information of the array data allows an accurate location of the scattering origin. The combination of high-resolution array processing and the scattering of $P'\bullet P'$

S. Rost (✉) · D.A. Frost
Institute of Geophysics and Tectonics, School of Earth and Environment, University of Leeds, Leeds LS2 9JT, UK
e-mail: s.rost@leeds.ac.uk

P.S. Earle
United States Geological Survey, DFC, MS 966, P.O. Box 25046, Denver, CO 80225, USA

P.M. Shearer
Institute of Geophysics and Planetary Physics, Scripps Institution of Oceanography, University of California, San Diego, USA

N.D. Selby
AWE Blacknest, Brimpton, Reading, UK

A. Khan and F. Deschamps (eds.), *The Earth's Heterogeneous Mantle*, Springer Geophysics, DOI 10.1007/978-3-319-15627-9_12

as probe for small-scale heterogeneities throughout the Earth's mantle will provide constraints on mantle convection, mantle structure, and mixing related to the subduction process.

Keywords Seismic scattering · Small-scale heterogeneity · Mantle mixing · Array seismology · Core–mantle processes

12.1 Introduction

Seismology aims to resolve structures on a wide variety of scale lengths from structures spanning several thousands of kilometers studied using earthquakes and tomographic techniques to the fine-scale structures resolved in industrial-style controlled source experiments allowing the resolution of structures on scales of just a few tens of meters (Fig. 12.1). The impressive high resolution of near-surface

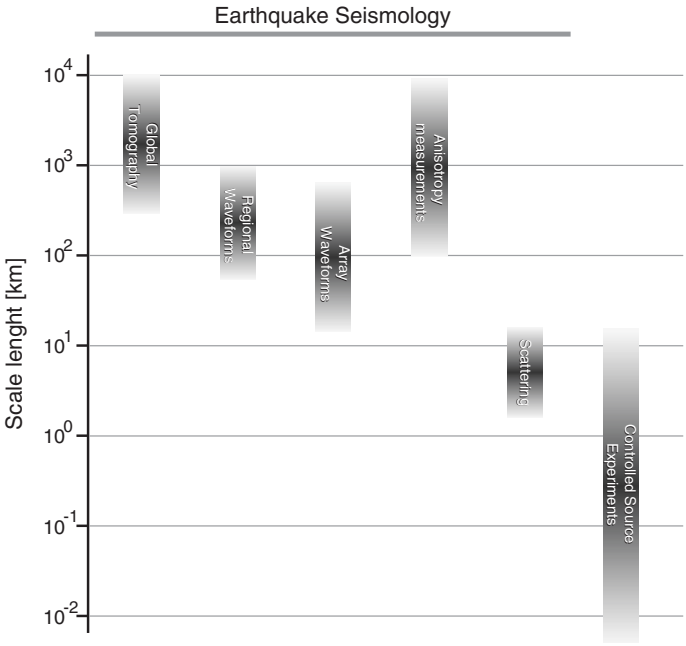

Fig. 12.1 Scale length sensitivity of different seismic probes for Earth structure. Seismic tomography resolves structures on a scale of a few hundred to a few thousand kilometers. Detailed waveform analysis using networks and arrays gives higher resolution information about Earth structure on scales as short as a few tens of kilometers. Scattering is sensitive to structure on the order of the seismic wavelength, which can reach a few kilometers in the short-period wavefield. Large-scale controlled source experiments can reach much higher resolution in the crust, but are impractical for studying the Earth's deep interior

controlled source experiments will likely always be beyond what can be achieved using global earthquake data, and only under particular circumstances is earthquake seismology able to resolve structures in the Earth's interior on scale lengths of tens of kilometers. On the other hand, geochemical analysis of mantle and crustal material typically reports heterogeneities in structure on scales as small as 10 m or less (Albarede 2005), while mineral physical studies report heterogeneities on scales comparable to the grain size and below (Stixrude and Lithgow-Bertelloni 2012). Clearly, there is a large discrepancy between the structures resolved by these disciplines studying the Earth's interior. Our understanding of the processes acting in the deep Earth and the dynamics and evolution of our planet is severely hampered by these fundamental differences in resolution.

Over the last few decades, global earthquake seismology has been very successful in mapping 3D deviations from the radially averaged 1D velocity structure that was established since the mid-twentieth century (Jeffreys and Bullen 1940; Bullen 1949; Dziewonski and Anderson 1981; Kennett and Engdahl 1991). These tomographic studies use the inversion of travel times (and to lesser extent waveforms) of seismic energy traveling along ray paths determined by the large-scale seismic velocity structure (Woodhouse and Dziewonski 1984). Nonetheless, the seismic wavefield, especially at higher frequencies, shows evidence for seismic energy not following the ray paths prescribed by the radial or large-scale seismic velocity structure. This energy, which is scattered into directions off the source–receiver plane at small-scale velocity or density variations, is most evident in the coda following the main arrivals or in dominant energy preceding certain arrivals. Codas trail the ray path traveling energy for several 10–100 s (Astiz et al. 1996; Rost et al. 2006) due to the longer path travelled by the scattered energy and seem to be incoherent between individual stations. Scattering at small-scale heterogeneities is dominant in the crust, and analysis of the coda of direct waves has widely been used to study crustal and lithospheric structure (Aki 1969; Korn 1988; Sato 1988). Nevertheless, seismic scattering has been shown to be a useful tool for studying the fine-scale structure of the Earth's deep interior (Shearer 2007).

Plate tectonics is constantly producing chemical heterogeneity through the generation of oceanic crust and the residual depleted mantle material, together forming the oceanic lithosphere, at mid-oceanic ridges and the subsequent recycling of the lithosphere into the Earth's mantle at subduction zones. The chemical heterogeneity between the crustal and mantle parts of the lithosphere is obvious from seismic studies of the crust, and seismic tomography indicates that the subducted material is traveling through the upper mantle, entering the lower mantle (Van der Hilst et al. 1991; Christensen and Hofmann 1994; Widiyantoro and Van der Hilst 1997; Li et al. 2008; McNamara and Zhong 2005; Tan and Gurnis 2005), although some slabs may remain in the upper mantle and transition zone (Fukao et al. 2009). The subducted material is likely slowly mixed into the ambient mantle (Allègre and Turcotte 1986; Olson et al. 1984) or might collect in larger volumes as indicated by tomographic studies and geodynamic modeling (Christensen and Hofmann 1994; McNamara and Zhong 2005). The mixing of the chemical heterogeneities of the subducted slabs likely leads to chemical heterogeneities throughout

the mantle. We expect a range of scale lengths for the heterogeneities based on the vigor of the mantle convection and the residence time of the heterogeneity (Olson et al. 1984). Such different scale lengths have been detected in seismic studies as discussed below. Geochemical and mineral physical analysis of surface samples have provided some evidence for this process, but the imaging of their structure in situ is essential for our understanding of the evolution, composition, and dynamics of the mantle. Analysis of the scattered seismic wavefield seems a good tool to detect, characterize, and map the chemical heterogeneities in the mantle and a start in closing the gap between seismology and other deep Earth geodisciplines.

The heterogeneities in the Earth's deep interior are likely much weaker than those found in the crust, and separating the weak scattering from the Earth's interior from the effects of the seismic wavefield traveling through the strong heterogeneities of the lithosphere beneath the station is difficult. Some parts of the seismic wavefield (Fig. 12.2) are particularly suited to studying deep Earth scattering. For these specific ray geometries, the scattered energy from the deep Earth can arrive as precursors to the main arrival traveling in the source–receiver plane and is therefore separated from the lithospheric scattering that dominates the coda after the main arrival. Therefore, these seismic phases provide valuable probes for examining the small-scale structure of the Earth's interior, as discussed in the next section. Here, we focus on scattering related to the *P*-wavefield. Although scattering has also been detected in a limited number of *S*-wave studies (Shearer 2007), their ability to detect the fine-scale structure of the Earth is limited due to the typically longer periods of teleseismic *S*-waves compared to *P*-waves, making the probes sensitive to different scale lengths.

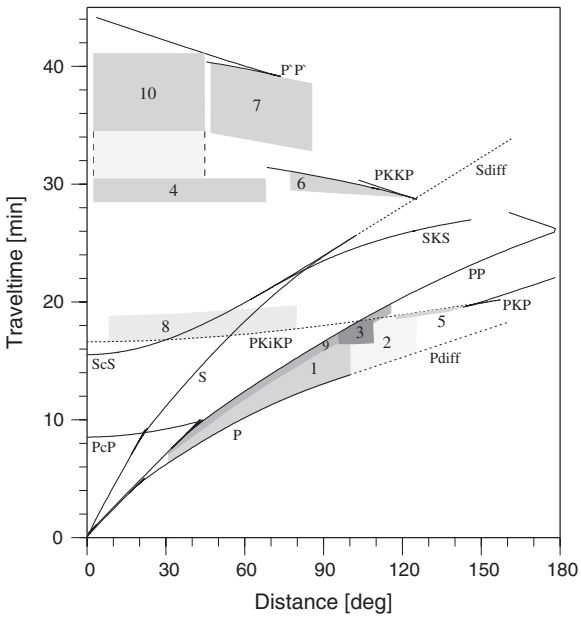

Fig. 12.2 Travel-time curves of common seismic body waves and theoretical time distance regions for several scattering probes: *1 P*-coda, *2* P_{diff} coda, *3* asymmetric *PP* precursors, *4 PK•KP* (precursors), *5 PKP* precursors, *6 PKKP* precursors, *7 P′P′* precursors, *8 PKiKP* coda, *9* symmetric *PP* precursors *10 P′•P′*. After Shearer (2007)

12.2 Scattering Probes

Due to the weak heterogeneity in the lowermost mantle compared to the lithosphere and the related change in the amplitude of the scattered energy, it is important to be able to separate the energy coming from these two scattering regions. To this end, several probes have been developed since the 1970s that allow good sampling of the lower mantle and close to the CMB.

12.2.1 PKP Precursors

PKP is a compressional wave that travels from the earthquake to the station as a *P*-wave through the mantle and core. The seismic velocity reduction at the CMB leads to a specific ray geometry where energy from the PKP_{bc} and PKP_{ab} branches, which travel through the outer core, is scattered close to the CMB and arrives as precursory energy to the *PKP* branch traversing the inner core (PKP_{df}). Ray paths for these branches are shown in Fig. 12.3a. Only scattering from heterogeneities in the deep Earth will arrive as PKP_{df} precursors. Due to the location of the *PKP b*-caustic, the point where the PKP_{bc} and PKP_{ab} paths merge, scattering up to approximately 1200 km above the CMB will produce precursors to PKP_{df} arriving up to 18 s before *PKP* and in an epicentral distance range from 118° to approximately 145°. These high-frequency arrivals have long been observed in the seismic wavefield (Gutenberg and Richter 1934), and their scattering origin was identified by Cleary and Haddon (1972). They have been used extensively to study scattering at the CMB to infer the structure of small-scale heterogeneities in the D″ region (Doornbos and Husebye 1972; Doornbos and Vlaar 1973; King et al. 1976; Bataille and Flatte 1988; Bataille et al. 1990; Hedlin et al. 1997; Thomas et al. 1999; Cormier 2000; Hedlin and Shearer 2000; Margerin and Nolet 2003; Cao and Romanowicz 2007; Vanacore et al. 2010). Heterogeneities higher above the CMB will not create precursors to PKP_{df} but will lead to energy with a longer travel time arriving as postcursors in the PKP_{df} coda. These are more difficult to analyze due to the simultaneously arriving energy scattered in the crust leading to a certain ambiguity in results (Hedlin and Shearer 2002) making the study of mid- and upper-mantle heterogeneity with this probe difficult.

Results have been interpreted in terms of CMB topography (Doornbos 1978) or small-scale heterogeneity close to the CMB (Haddon and Cleary 1974). Heterogeneities have been found to consist of ~1 % root-mean-square (RMS) velocity variations at scale lengths of about 8 km in a layer of several hundred kilometers thick (Bataille and Flatte 1988; Hedlin et al. 1997), although there is some trade-off between the thickness and the heterogeneity strength and recent studies report a much smaller RMS variation (Mancinelli and Shearer 2013). Alternatively, the scattering has been attributed to CMB topography with RMS

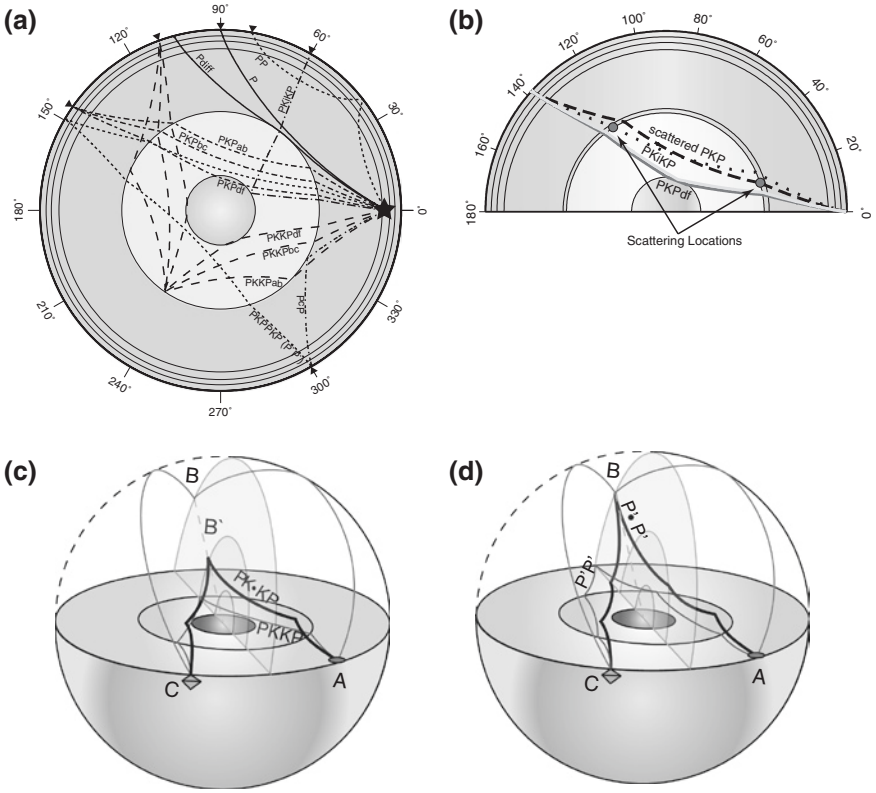

Fig. 12.3 **a** Ray paths of *PKP*, *PKiKP*, *PP*, *PKKP*, $P'P'$, P/P_{diff}, and *PcP*, all of which, have been used to study scattering in the Earth's interior. Source (star) is located at 500 km depth, and receiving stations are indicated by inverted triangles. **b** Scattered ray path related to *PKP*, producing precursors to PKP_{df}, an often-used probe for lower mantle scattering. **c** Scattered ray path (*dark solid*) related to *PKKP* (*light gray* ray path) with a scattering point (B') on the CMB at the *PKKP* CMB reflection point. Point *B* marks the surface projection of the scattering point B'. *PK•KP* scattered energy is traveling off-azimuth. The globe is cut along the *PKKP* ray path traveling on-azimuth [i.e., along the great-circle path connecting source (*A*) with receiver (*C*)]. Please note that a second mirrored scattering point can be found in the lower hemisphere. **d** Scattered ray path (*dark* ray path) related to *PKPPKP* ($P'P'$) (*light gray* ray path). Scattering is indicated near the surface at point *B*, and the scattered energy is traveling off-azimuth. The globe is cut along the *PKPPKP* ray path traveling on-azimuth between source (*A*) and receiver (*C*). Please note that a second mirrored scattering point can be found in the lower hemisphere

height of ~300 m (Bataille et al. 1990). A second group of studies located discrete scatterers at the CMB rather than treating the scattering as a statistical process (Thomas et al. 1999; Frost et al. 2013). Resolving heterogeneities high above the CMB with *PKP* is challenging, but this gap can be closed using other phases as described below.

12.2.2 *P* and P_{diff} Coda

At distances larger than about 98°, the direct *P*-wave starts to diffract around the low-velocity zone of the outer core (Fig. 12.3a). This diffracted energy is typically called P_{diff} and can be observed, in the high-frequency seismic wavefield, out to at least 115°, although it might disappear earlier (Astiz et al. 1996; Rost et al. 2006) and some observations out to 130° have been reported likely due to wave guide effects (Bataille et al. 1990; Earle and Shearer 2001). P_{diff} is often followed by long coda energy trailing the main arrival for several hundred seconds (Astiz et al. 1996; Rost et al. 2006). At large ranges, the arrivals seem emergent, reaching maximum amplitudes up to tens of seconds after the main *P* or P_{diff} arrival. The length of the coda and its emergent onset support the interpretation of the P_{diff} coda originating from multiple scattering along the diffracted path (Bataille et al. 1990). A global stack of short-period seismograms from shallow events by Earle and Shearer (2001) found evidence for 1 % RMS velocity variations on scale lengths of 2 km, smaller than generally resolved by *PKP* studies. Strong regional variations in the strength of the coda have also been observed (Rost and Thorne 2010) indicating lateral variations in scattering strength.

12.2.3 *PKKP* and $P'P'$

Core phases other than *PKP* have been used to study scattering in the deep Earth. Scattering related to *PKKP*, a core phase reflected once off the underside of the CMB (Fig. 12.3a), has been identified in several distance ranges. Early studies identified precursors to $PKKP_{\mathrm{df}}$ between ~80° and 125° (Doornbos 1974; Earle and Shearer 1997) and have been interpreted as scattering at the CMB entry or exit points (*PKK•P* or *P•KKP*, where • denotes the location of the scattering along the ray path). The scattering process is analogous to the scattering of PKP_{bc} or PKP_{ab} leading to PKP_{df} precursors as described above with an additional reflection of the energy from the underside of the CMB. In the case of *PKKP,* most studies point toward scattering from small-scale CMB topography or roughness with amplitudes of 250–350 m on lateral scales of 7–10 km (Earle and Shearer 1997). *PKKP* scattering at distances shorter than 80° has also been detected in global stacks (Earle and Shearer 1998). The origin of this energy has later been identified as scattering of *P* to *PKP* (*P•PKP*) at the Earth's surface (Earle 2002).

An additional scattering mechanism for *PKKP* has been identified by Earle (2002) as scattering of *PKKP* at the CMB reflection point (*PK•KP*). This scattering is related to off-azimuth scattering of $PKKP_{\mathrm{bc}}$ off volumetric heterogeneities at or above the CMB (Fig. 12.3c). This scattering geometry has been used to map lateral heterogeneities of scattering strength at the CMB and to find evidence for discrete heterogeneities likely related to subduction processes and heterogeneities at the edges of the large low shear velocity Provinces (LLSVPs) beneath the Pacific and Africa (Rost and Earle 2010).

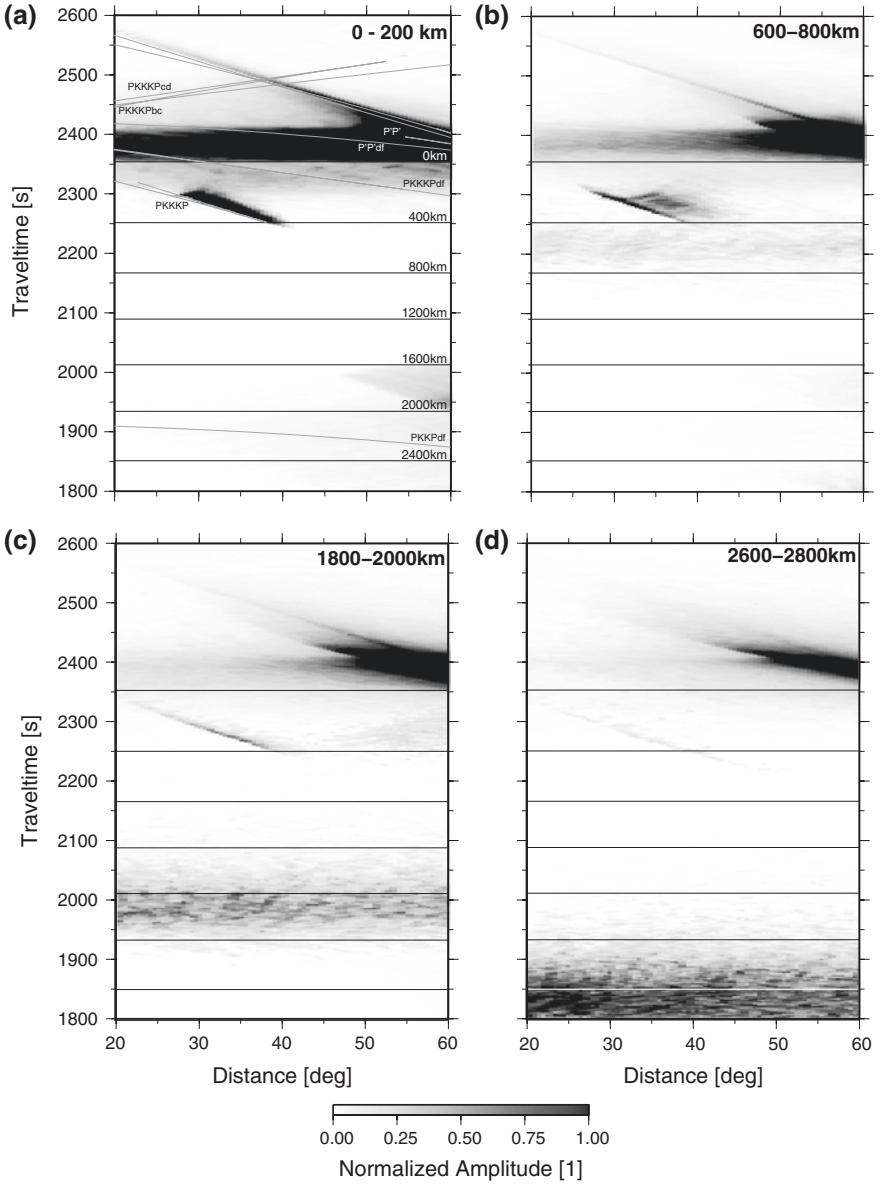

Fig. 12.4 Synthetic wavefields calculated using a Monte-Carlo phonon scattering approach (Shearer and Earle 2004, 2008). The wavefield runs from 1800 to 2600 s after the earthquake origin time and covers a distance range from 20° to 60°. Some of the main arrivals including different branches of *PKKKP* and $P'P'$ (*PKPPKP*) are marked in **a**. Amplitudes are normalized to the maximum amplitude in each individual panel. Horizontal lines mark the minimum arrival times for scattering related to $P'P'$ ($P'\bullet P'$) from the surface to the D″ region. **a** Scattering in a 200 km thick layer ranging from 0 to 200 km depth with RMS velocity variations of 3 % with 4 km correlation length characterized in an exponential autocorrelation model. **b** As **a**, but for a layer ranging from 600 to 800 km depth. **c** As **a** but for a layer ranging from 1800 to 2000 km depth. **d** As **a** but for a layer ranging from 2600 to 2800 km depth. Variations in scattering amplitude are due to the normalization of each panel

PKPPKP ($P'P'$) is similar to *PKKP* as it is an underside reflection off the Earth's surface (Fig. 12.3a), while *PKKP* is an underside reflection off the CMB. Scattering related to $P'P'$ has been identified in near-podal array data (Tkalčić et al. 2006), and its timing indicates a source in the upper mantle between 150 and 220 km depth.

It has been shown that the time window from 2200 to 2500 s after the earthquake origin time for distance ranges of 30°–50° contains scattered energy related to the phase $P'P'$. Earle et al. (2011) identify this energy as off-great-circle path scattering of PKP_{bc} to PKP_{bc} ($P'\bullet P'$). The travel time of $P'\bullet P'$ is dependent on the scattering depth (Fig. 12.4) with energy scattered closer to the CMB arriving earlier in the seismogram (Earle et al. 2011). This makes $P'\bullet P'$ an ideal probe to study small-scale heterogeneity from crust to core and a good supplement to scattering studies using *PKP* for which energy scattered at heterogeneities more than about 1000 km above the CMB arrives in the PKP_{df} coda, making the analysis of this energy more complex (Hedlin and Shearer 2002). With this scattering mechanism, *PK•KP* is an extreme example of lowermost mantle scattering of $P'\bullet P'$ explaining the sensitivity of *PK•KP* to structure above the CMB. Here, we show evidence for mapping of whole mantle scattering using $P'\bullet P'$ in the next section.

12.2.4 Other Probes (P, PcP, PP)

Other phases have been used to delineate heterogeneities at different depths throughout the Earth. Arrivals in the *P*-coda, identified as *S*-to-*P* conversions close to the source or *P*-to-*P* scattering off azimuth, have been used to map structure in the mid-mantle through analysis of array data (Castle and Creager 1999; Kaneshima and Helffrich 1999, 2003; Kaneshima 2009; Kaneshima et al. 2010; Kito et al. 2008). These detections are generally in the vicinity of current or recent subduction, outlining the penetration of slabs into the lower mantle and the recycling or deposition of crustal material in the lowermost mantle.

A similar result has been obtained by studying precursors to *PP*. The *PP* precursor wavefield shows evidence for symmetric reflections off the upper-mantle discontinuities (Shearer 1990) and for asymmetric reflections off the surface or uppermost mantle (Wright 1972; King et al. 1975; Weber and Wicks 1996). Asymmetric off-azimuth reflections off slab material arriving as *PP* precursors have been identified beneath the Mariana and Izu-Bonin subduction zones (Rost et al. 2008; Bentham and Rost 2014), outlining deep subduction beneath these subduction zones and the transport of oceanic crust far into the lower mantle. Other phases such as *PcP* have been used to image lower mantle structure through the analysis of *P*-to-*P* and *S*-to-*P* scattering (Braña and Helffrich 2004).

The outer core seems well mixed and does not show evidence for scattering away from the boundaries between mantle and core (CMB) and inner and outer core (ICB). On the other hand, there is strong evidence from the analysis of *P*-waves traversing the inner core for scattering in the inner core indicating heterogeneities of up to 1.2 % in velocity and scale lengths of 2 km in the outermost

300 km (Cormier 2007; Koper et al. 2004; Leyton and Koper 2007; Poupinet and Kennett 2004; Rost and Garnero 2004; Vidale and Earle 2000; Vidale et al. 2000). These heterogeneities are likely due to inclusion of melt in the solid core, compositional changes, or changes in the anisotropy of the core material (Vidale and Earle 2000).

12.3 *P′•P′/PK•KP* and Earth Structure

Scattering related to $P'P'$ ($P'•P'$) has been identified in data of the Large Aperture Seismic array (LASA), an array of up to 625 station with an aperture of 200 km that operated in Montana from 1965 to 1978 (Earle et al. 2011). The energy, arriving at epicentral distances of 30°–50° and at times between 2300 and 2450 s after the earthquake origin, has been interpreted as off-azimuth scattering of PKP_{bc} to PKP_{bc} (Earle et al. 2011). The scattered energy recorded at the array shows a distinct off-azimuth energy pattern similar to the precursors to *PKKP* described earlier (Earle 2002; Rost and Earle 2010). Note that $P'•P'$ differs from $P'P'$ precursors (Fig. 12.2), which are related to underside reflections off discontinuities and through scattering at the surface reflection point and arrive primarily along the great-circle path (Cleary and Haddon 1972; Haddon et al. 1977; Chang and Cleary 1981; Cleary 1981; Tkalčić et al. 2006). The energy of $P'•P'$ travels off-azimuth (i.e., the azimuth connecting source and receiver) around the inner core leading to up to two characteristic energy peaks (depending on the existence of heterogeneity in the potential scattering region) with nonzero transverse and radial slowness, indicating a CMB, lower mantle, or outer-core origin (Fig. 12.5a). The characteristic energy pattern derived using ray theory can also be identified in simulations of global seismic scattering. Figure 12.5b, c shows examples of scattered energy in a time window from 1950 to 2000 s for distance ranges of 30°–35° (Fig. 12.5b) and 40°–45° (Fig. 12.5c). Synthetics are calculated using a multiple scattering, Monte-Carlo phonon scattering approach (Shearer and Earle 2004), and the resulting energy peaks are in good agreement with the ray theoretical calculations (Earle et al. 2011).

Here, we detect the energy related to $P'•P'$ in data of the medium aperture array in Yellowknife (YKA) located in northern Canada. YKA consists of 18 short-period, vertical stations deployed along two perpendicular north–south and east–west oriented legs. The maximum aperture of the array is 20 km with an interstation spacing of 2.5 km. YKA was designed to detect high-frequency *P*-waves from underground nuclear explosions (Manchee and Weichert 1968; Weichert and Whitham 1969) and is therefore well suited to study the scattered *P*-wavefield. Additionally, YKA contains 4–5 three-component broadband seismometers, but the data from these instruments are not being used in this study. Earle et al. (2011) identified $P'•P'$ in data from LASA consisting of more than 600 seismometers and with an aperture of up to 200 km (Frosch and Green 1966;

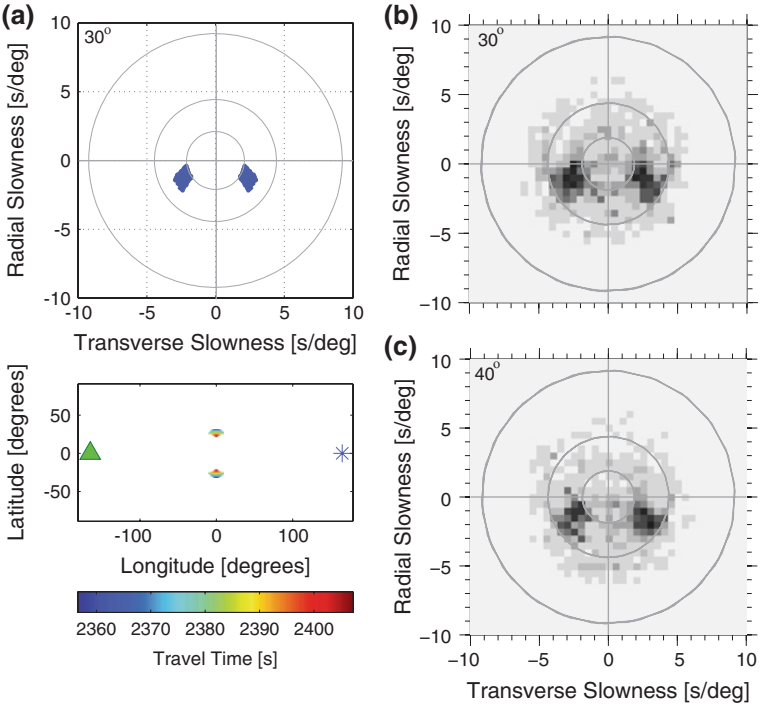

Fig. 12.5 **a** Theoretical calculation of expected slowness patterns for $P'•P'$ (*top*) and travel times of scattered energy from two locations symmetrically off-azimuth (*bottom*). *Color scale* indicates travel time for scattering energy within the scattering regions. For scattering regions see also Fig. 12.3. Travel times are calculated for scattering at the surface and for a distance of 30° between source (*star*) and receiver (*triangle*). *Blue areas* in *top panel* indicate the slowness region where scattered energy for this source-receiver constellation can originate from. **b** Slowness pattern of scattered energy calculated for a distance range from 30° to 35° and in the time windows from 1950 to 2000 s after origin. Synthetics have been calculated using a Monte-Carlo phonon scattering approach (Shearer and Earle 2004). The model includes heterogeneities with RMS velocity variations of 3 % with an exponential autocorrelation length of 4 km in a 200-km-thick layer between 1800 and 2000 km depth. Two energy lobes in agreement with the theoretical calculations are visible. The difference in travel times of the scattered energy relative to **a** is due to the different scattering depth (see Fig. 12.4). **c** As in **b** but for an epicentral distance from 40° to 45°. The panels in **b** and **c** indicate the slight changes in slowness pattern of the scattered energy

Green et al. 1965). LASA therefore has much better resolution in wave number space and provides greater improvements in the signal-to-noise ratio of coherent arrivals. Here, we show the capability of smaller arrays to detect $P'•P'$, opening up many more opportunities to use this energy to study Earth structure. Further testing will see whether smaller arrays than YKA (with apertures of 3–10 km, which have been built as part of the Comprehensive Test Ban Treaty) are able to detect the weak scattered energy related to $P'•P'$.

To enhance detection of coherent signal power in the stacked array data and increase resolution in slowness space, we apply the *F*-statistic to the array beams (Selby 2011; Frost et al. 2013). To detect the weak scattered energy related to $P'•P,'$ we perform a grid search over slowness (ranging from 0 to 13 s/°) and backazimuth (from 0° to 360°). For each slowness/backazimuth combination, we form the array beam and apply the *F*-statistic, which is a dimensionless measure of the beampower divided by the variability (difference) between the beam and each individual trace contributing to the beam average over a time window of specified length. The maximum amplitude of this *F*-trace is then measured in a time window representing a specific scattering depth as discussed below. The resulting slowness/backazimuth *F*-trace beampower maps (*F*-packs) indicate the slowness and backazimuth of the incoming energy with high precision (Frost et al. 2013). The use of the *F*-statistic penalizes energy traveling with incidence angles other than the one the beam is calculated for, therefore sharpening the array response function and the wave number resolution of the array, while improving the signal-to-noise ratio of the energy traveling along the correct slowness vector.

We selected a small dataset of events with magnitude larger than 6.5 and good signal-to-noise ratio from the YKA data holdings (Fig. 12.6). Most earthquakes form two groups located beneath Kamchatka and Central America. We apply the *F*-trace stacking approach to 50-s time windows of the YKA data. Each time window represents an approximately 200-km-thick layer in the Earth. We move our analysis from the surface to the CMB (see Table 12.1 for chosen time windows). As can be seen in Fig. 12.4, each of these time slices represents scattering from a specific depth, making $P'•P'$ an ideal probe to study the small-scale heterogeneity

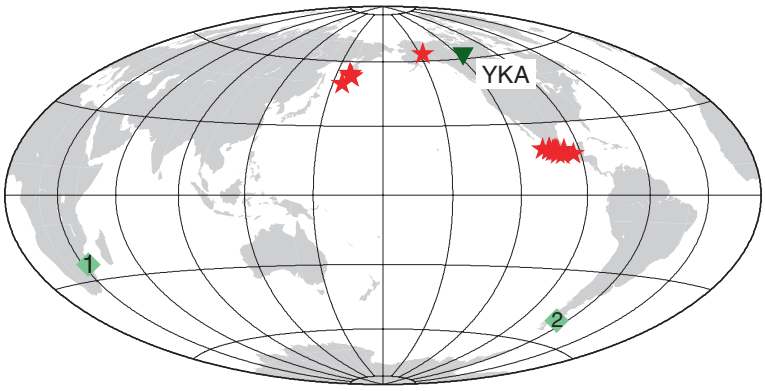

Fig. 12.6 Location of events (*stars*) analyzed in this study. The events fall into two general areas with events beneath Kamchatka and Central America. *Diamonds* show scattering regions of example event (January 28, 2002, 13:50) shown in Fig. 12.7 with the *green diamond* marked *1* showing the location in the deep mantle and the upper mantle scattering point is shown as *green circle* marked *2*

Table 12.1 Minimum travel times for $P'•d•P'$ scattered phases for varying scattering depths for the one-dimensional Earth model PREM (Dziewonski and Anderson 1981)

Scattering depth (km)	PREM	
	PKP caustic distance (°)	Minimum $P'dP'$ travel time (s)
0	145.05	2353.48
200	144.59	2300.36
400	144.05	2252.28
600	143.38	2208.40
800	142.55	2167.90
1200	140.49	2090.36
1600	137.87	2014.08
2000	134.44	1938.04
2400	129.46	1854.36
2600	126.14	1809.50
2800	121.40	1756.14

Time indicates absolute travel time after the origin for a surface focus. Also given is the PKP_b caustic distance for the appropriate scattering depth

from crust to core. The scattered energy from all these time windows arrives in a quiet time window with few interfering phases (*PKKKP*, with two CMB underside reflections, is the only major phase arriving in the $P'•P'$ scattering time window, also see Figs. 12.2 and 12.4 and might be visible as on-azimuth arrival in the 200–400 km and 400–600 km depth slices in Fig. 12.8). Figures 12.7 and 12.8 show the resulting energy maps for the packed *F*-beams for the individual time windows for two example events. The energy maps show discrete and coherent $P'•P'$ arrivals for the upper mantle (down to depths of about 400 km) and in the lowermost mantle to depths of about 900 km above the CMB (below 2000 km depth) with slowness patterns that are in excellent agreement with the ray theoretical and phonon scattering synthetics. The example event in Fig. 12.8 shows the typical two-lobed scattered energy in the uppermost mantle slice. We interpret this energy as detection of $P'•P'$ in the YKA data. *F*-packs from the mid-mantle indicate little scattered $P'•P'$ energy from depths of about 600–2000 km, as indicated by the absence of a focussed arrival (as, e.g., in the shallower depth slices) and a more incoherent wavefield indicating varying slowness and backazimuth in the processed time window. Tests with noise windows before the *P* arrival for these events show a random behavior of the energy maximum in these time windows, while the *F*-packs between 600 and 2000 km depth often show a predominant direction in agreement with scattering and outer core slowness, but indicating very low scattered energy. This might indicate that there is some scattered energy arriving in these time windows, but is much weaker than at the surface and in the lower mantle. Detailed modeling of this energy related to the YKA noise condition will lead to further insight into the strength of the heterogeneities at these depths but is beyond the scope of this study. The dataset studied here consists of seismicity

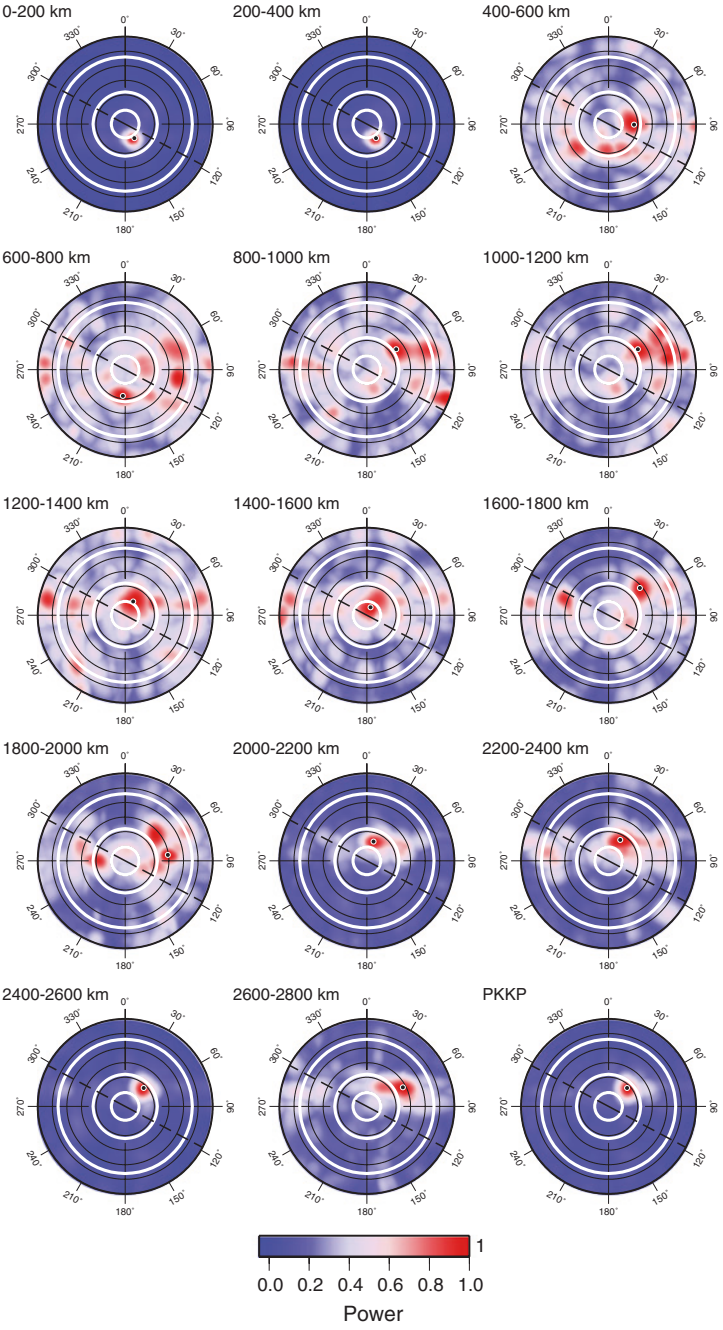
0-200 km
200-400 km
400-600 km
600-800 km
800-1000 km
1000-1200 km
1200-1400 km
1400-1600 km
1600-1800 km
1800-2000 km
2000-2200 km
2200-2400 km
2400-2600 km
2600-2800 km
PKKP
0.0 0.2 0.4 0.6 0.8 1.0
1
Power

Fig. 12.7 *F*-packs, examples for the event January 28, 2002, 13:50 in the Kamchatka region recorded at YKA. Epicentral distance for this event is 47.7°. In each *F*-pack plot, slowness is shown on the radial and backazimuth of the incident energy on the azimuthal axes. *Black circles* indicate slowness at intervals of 2 s/°. *Thick white circles* indicate slowness of 1.9, 4.4, and 9.2 s/°, indicating energy originating from the inner-core boundary, core–mantle boundary, and 660-km discontinuity, respectively. Colors indicate beampower of the *F*-beams, with each panel being normalized individually. Focussed, high beampower (as in slices for 0–200 and 200–400 km) indicates very coherent energy arriving from the related slowness and backazimuth, while distributed (non-focussed) energy from different slowness and backazimuths indicates the arrival of uncorrelated noise (as in slices from 400 to 2000 km depth). *Dashed black lines* indicate the theoretical backazimuth for this event of 297.9°. Depth slice time windows relate to Table 12.1, and the *PKKP*-labeled time window contains energy originating from the CMB (time window between 1651 and 1751 s)

beneath Kamchatka and Central America. We find that in general, the events in the Kamchatka region show evidence for scattering throughout most of the mantle (although with apparently weaker scattering in the mid-mantle), while the Central American events show only evidence for scattered energy from the upper mantle (see Fig. 12.9 for an example). This might indicate lateral variations in heterogeneity structure in the lower mantle as has been indicated before (Hedlin and Shearer 2000). Note that the lower mantle scattering (e.g., Fig. 12.7) shows different slowness and backazimuth parameters than the upper-mantle scattering in the same event. The different directivity for the scattered energy indicates different locations of the heterogeneities leading to the scattered energy. Using the slowness/backazimuth information and raytracing through a 1D Earth model allows us to infer the location of these heterogeneities. The lower mantle scattering originates from the edge of the large low shear velocity province (LLSVP) beneath Africa (scattering region 1 in Fig. 12.6 (see also Fig. 12.10)), a region of strong reductions in seismic velocities beneath Africa. Another LLSVP can be found beneath the Pacific, and combined, they form a strong degree 2 pattern of low velocities in most tomographic models (Garnero and McNamara 2008). Strong scattering from the edge of the LLSVP has been reported earlier (Wen 2000; Rost and Earle 2010; Frost et al. 2013). On the other hand, we can relocate the near-surface scattering to a region beneath South America (scattering region 2 in Fig. 12.6) where the upper mantle is strongly influenced by recent subduction. Several events from a similar source region support the detection of these scattering regions.

As shown in Figs. 12.7, 12.8 and 12.9, $P'•P'$ offers a unique opportunity to probe the mantle, from crust to core, for small-scale heterogeneities using scattered waves. Due to the complex ray path of $P'•P'$ and the location of most seismic arrays on the Northern Hemisphere, we expect the best sampling with this probe on the Southern Hemisphere. This will be a good complement to previous studies probing for heterogeneities close to the CMB using *PKP* (Hedlin and Shearer 2000).

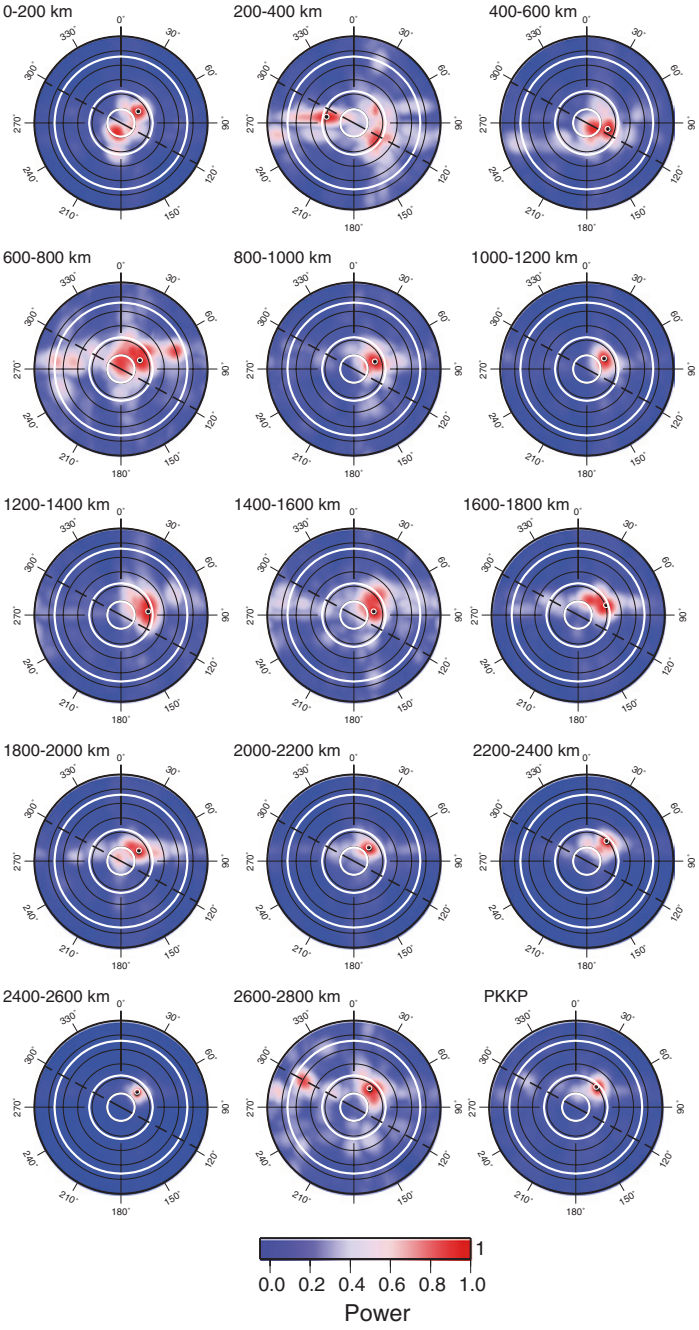
0-200 km
200-400 km
400-600 km
600-800 km
800-1000 km
1000-1200 km
1200-1400 km
1400-1600 km
1600-1800 km
1800-2000 km
2000-2200 km
2200-2400 km
2400-2600 km
2600-2800 km
PKKP
0.0 0.2 0.4 0.6 0.8 1.0
1
Power

Fig. 12.8 *F*-packs, examples for the event March 02, 1992, 12:29 in the Kamchatka region recorded at YKA. Epicentral distance for this event is 43.2°. In each *F*-pack, plot slowness is shown on the radial and backazimuth of the incident energy on the azimuthal axes. *Black circles* indicate slowness at intervals of 2 s/°. *Thick white circles* indicate slowness of 1.9, 4.4, and 9.2 s/°, indicating energy originating from the inner-core boundary, core–mantle boundary, and 660-km discontinuity, respectively. *Red colors* show high beampower of the *F*-beams indicating very coherent energy arriving from the related slowness and backazimuth. *Dashed black lines* indicate the theoretical backazimuth for this event of 298.3°. Depth slice time windows relate to Table 12.1, and the *PKKP*-labeled time window contains energy originating from the CMB (time window between 1651 and 1751 s)

A special case of the energy related to *P′•P′* is *PKKP* scattered energy from heterogeneities close to the CMB (*PK•KP*) as described above. This energy has been detected in both data from large aperture (Earle and Shearer 1997; Earle 2002) and medium aperture (Rost and Earle 2010) arrays. It has been used to study the lateral variations of heterogeneities along the Earth's CMB (Rost and Earle 2010). Figure 12.10 shows detected discrete scatterer locations for *PK•KP* from an earlier study (Rost and Earle 2010) and compares the locations with velocity variations derived from tomographic studies. The scatterer locations can predominantly be found at the edge of the African LLSVP, in agreement with other studies (Hedlin and Shearer 2000; Wen 2000; Frost et al. 2013) and beneath Central and South America. While the LLSVP region is seismically slow and has been interpreted as a thermochemical pile (McNamara and Zhong 2005), the other dominant scatterer region is characterized by fast seismic velocities (Fig. 12.10b). These regions are likely related to the long-lasting subduction beneath the Americas (Lithgow-Bertelloni and Richards 1998). Further scattering points, but much fewer than in these two regions, can be found in the Pacific LLSVP and in the circum-Pacific subduction ring. Together, the *P′•P′ and PK•KP* results indicate a dynamic structure of the lower mantle, where convection flows redistribute small-scale heterogeneities.

The heterogeneities from the two dominating scattering areas beneath Africa and Patagonia are likely generated by different processes. Newly introduced subducted material is likely producing the heterogeneity beneath South America. The scattering area detected beneath Patagonia agrees well with the inferred location of the Phoenix plate at the CMB (Lithgow-Bertelloni and Richards 1998). Ultra-low velocity zones (ULVZs), regions of strongly reduced seismic velocities at the CMB (Garnero 2000), have been predominantly found at the edges of LLSVPs (McNamara et al. 2010). Geodynamic modeling of the lowermost mantle indicates that dense material is likely deposited at the edges of thermochemical piles in agreement with ULVZ detection (McNamara et al. 2010). It seems possible that the heterogeneities leading to scattering at the edge of the LLSVP beneath Africa are related to dense material swept to the edge of LLSVPs by the internal convection currents of the LLSVPs. Detailed modeling of scattering from structures derived from geodynamic models might lead to better insight into these processes but is beyond the scope of this paper.

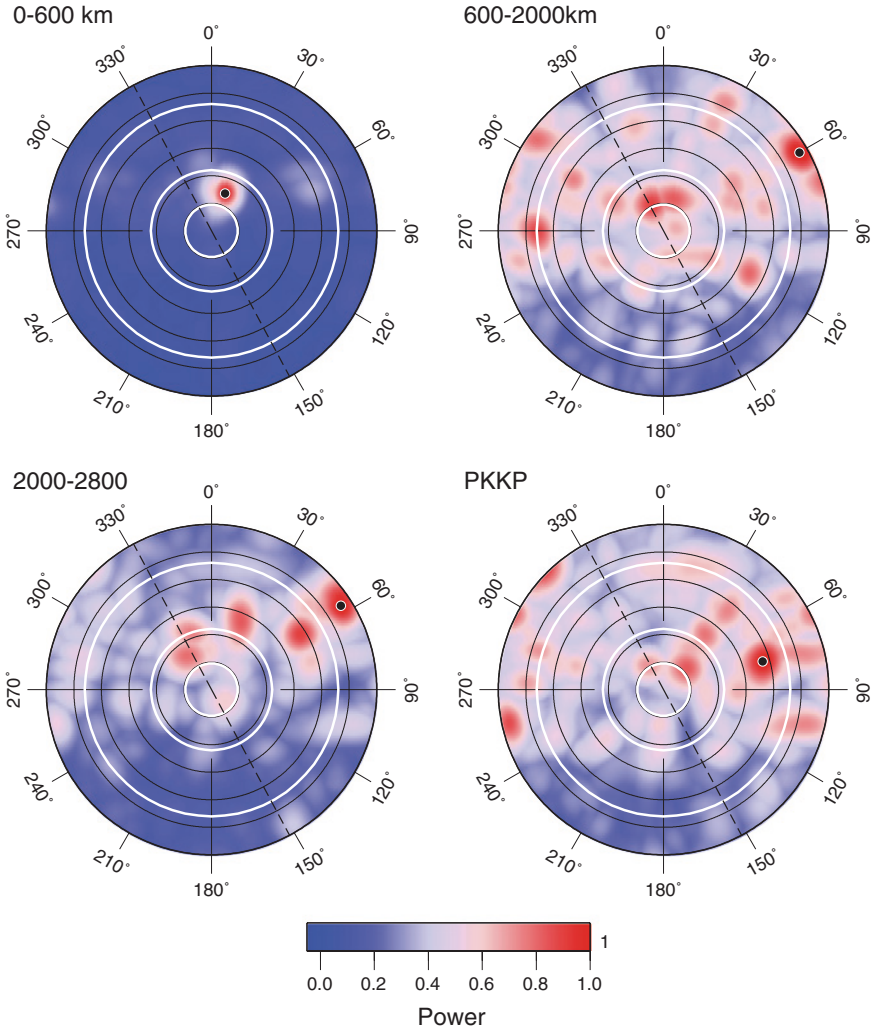

Fig. 12.9 *F*-pack results for the event October 21, 1995, 02:38 in Central America recorded at YKA with an epicentral distance of 48° and a backazimuth of 151.86° (*dashed line*). *F*-packs are shown in larger slices running from 0 to 600 km (*top left*), 600 to 2000 km (*top right*), 2000 to 2800 km (*bottom left*), and the PKKP time window (*bottom right*). *F*-packs are shown in the same way as in Fig. 12.7. Only the upper mantle time slice (*top left*) shows coherent scattering, while the other depth slices indicate mostly incoherent noise in contrast to the examples shown in Figs. 12.7 and 12.8

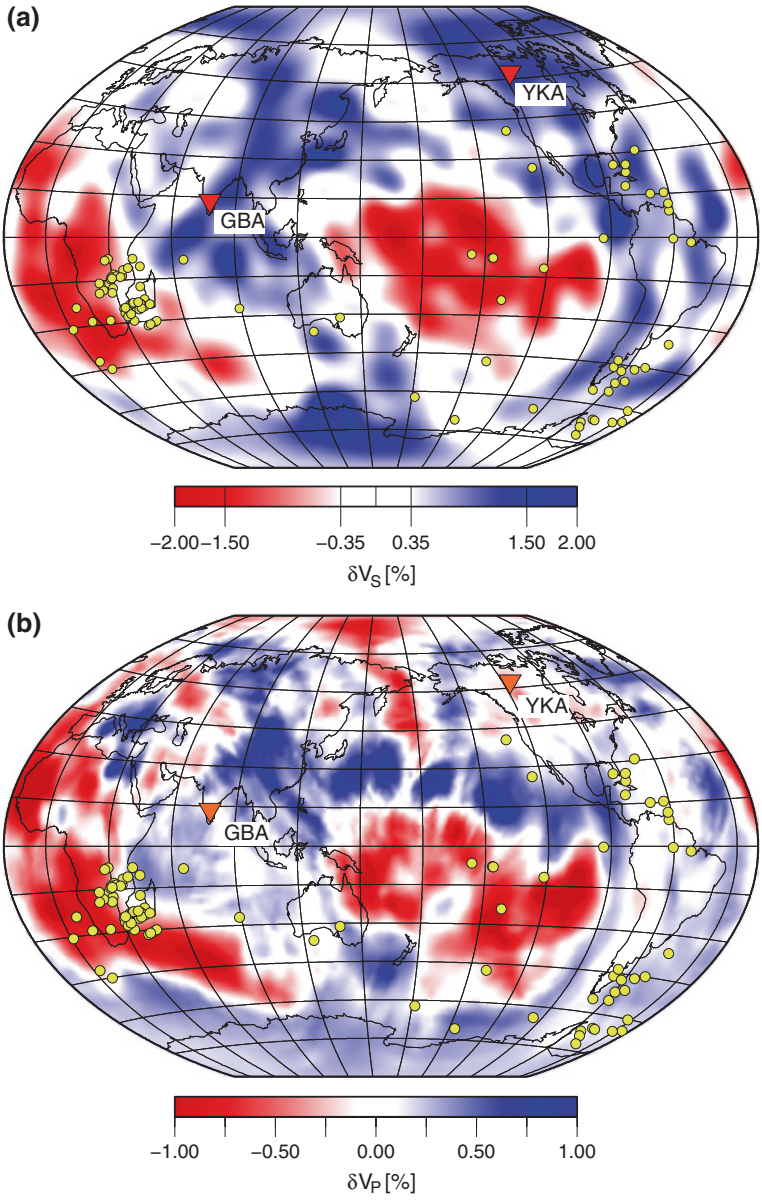

Fig. 12.10 Scatterer locations (*yellow circles*) at the CMB as found in data from 2 medium aperture arrays (*red triangles*) located in Canada (YKA) and India (GBA) (Rost and Earle 2010). **a** Background shows *S*-wave velocity at the CMB from Ritsema et al. (2011). **b** Background shows *P*-wave velocity variations from LLNL_G3Dv3 (Simmons et al. 2012)

12.4 Conclusion

Scattering from small-scale heterogeneities in the Earth is evident in the short-period seismic wavefield and provides us with the best opportunity to learn about the small-scale structure of the planet's interior. Scattering has now been detected at most depths throughout Earth, with the well-mixed outer core currently being the only exception. Although many details of this small-scale structure remain poorly resolved, new probes to small-scale heterogeneities, as discussed in this work, offer the opportunity to gather more information about the fine structure of the Earth. The existence of strong scatterers close to the top and the bottom of the convecting mantle, i.e., close to the boundary layers of the convection system, is probably expected. Nonetheless, the data studied here provide constraints on the dominant flow in the mantle and the mixing processes that tend to homogenize the mantle (Olson et al. 1984).

This preliminary study of $P'•P'$ shows that the upper mantle and lower mantle produce strong scattering, while the scattering from the mid-mantle seems much weaker. There is also evidence for lateral variations in the heterogeneity structure as evidenced by the absence of scattering from the lower mantle in the Central American earthquakes. The heterogeneities leading to the scattering are likely compositional since the high thermal diffusivity in the solid mantle would equalize the thermal anomaly of a 10 km heterogeneity on the order of 200 kyrs (Helffrich and Wood 2001). An obvious source for the compositional heterogeneities is the subduction process, continuously adding depleted and enriched crustal and lithospheric material to the bulk mantle, which has been identified as a possible source for seismic scattering (Helffrich and Wood 2001). Recent tomographic images show that subducting slabs in many regions do not penetrate the 660-km discontinuity and remain in the upper mantle and transition zone, while others continue to travel into the lower mantle therefore depositing chemical heterogeneities close to the CMB (Simmons et al. 2012). The upper mantle beneath South America has been found to be seismically fast indicating the existence of slab material being trapped in the upper mantle (Simmons et al. 2012). This is in good agreement with the strong scattering detected by $P'•P'$.

LLSVPs have been speculated to be either primordial or being recharged through the subducted crustal material (Garnero and McNamara 2008) although the latter has been questioned recently (Deschamps et al. 2012). Either model predicts strong structure in the LLSVPs related to the internal convection (McNamara et al. 2010). This is in good agreement with the laterally varying scattering strength close to the CMB as found in the *PK•KP* data. Although topography on the CMB has been used to explain the scattering in earlier studies (Doornbos 1978), it has been found that it cannot explain global *PKKP* scattering (Earle and Shearer 1997) and cannot explain the $P'•P'$ scattering located away from the CMB presented here.

The new probes to small-scale heterogeneities, $P'•P'$ and *PK•KP*, presented here and the rapid increase in dense array deployments will allow a systematic exploration of much of the Earth's mantle for small-scale heterogeneities. Using

the seismic observations of scattering in the high-frequency wavefield and refined thermochemical convection models will provide further insight into the generation, distribution, and destruction of chemical heterogeneities from mixing processes in the mantle.

References

Aki K (1969) Analysis of seismic coda of local earthquakes as scattered waves. J Geophys Res 74(2):615–631

Albarede F (2005) The survival of mantle geochemical heterogeneities. Earth's Deep Mantle Struct Compos Evol 160:27–46. doi:10.1029/160GM04

Allègre CJ, Turcotte DL (1986) Implications of a two-component marble-cake mantle. Nature 323(6084):123–127. doi:10.1038/323123a0

Astiz L, Earle P, Shearer P (1996) Global stacking of broadband seismograms. Seism Res Lett 67(4):8–18. doi:10.1785/gssrl.67.4.8

Bataille K, Flatte S (1988) Inhomogeneities near the core-mantle boundary inferred from short-period scattered *PKP* waves recorded at the global digital seismograph network. J Geophys Res 93(B12):15057–15064. doi:10.1029/JB093iB12p15057

Bataille K, Wu R, Flatte S (1990) Inhomogeneities near the core-mantle boundary evidenced from scattered waves—a review. Pure Appl Geoph 132(1–2):151–173

Bentham HLM, Rost S (2014) Scattering beneath Western Pacific subduction zones: evidence for oceanic crust in the mid-mantle. Geophys J Int 197:1627–1641

Braña L, Helffrich G (2004) A scattering region near the core-mantle boundary under the North Atlantic. Geophys J Int 158(2):625–636

Bullen K (1949) An Earth model based on a compressibility-pressure hypothesis. Month Not R Astr Soc 109(6):720–720

Cao A, Romanowicz B (2007) Locating scatterers in the mantle using array analysis of PKP precursors from an earthquake doublet. Earth Planet Sci Lett 255(1–2):22–31

Castle JC, Creager KC (1999) A steeply dipping discontinuity in the lower mantle beneath Izu-Bonin. J Geophys Res 104(B4):7279–7292. doi:10.1029/1999JB900011

Chang A, Cleary J (1981) Scattered PKKP—further evidence for scattering at a rough core-mantle boundary. Phys Earth Planet Inter 24(1):15–29

Christensen U, Hofmann A (1994) Segregation of subducted oceanic-crust in the convecting mantle. J Geophys Res 99(B10):19867–19884

Cleary J (1981) Seismic-wave scattering on underside reflection at the core-mantle boundary. Phys Earth Planet Inter 26(4):266–267

Cleary J, Haddon R (1972) Seismic wave scattering near core-mantle boundary—new interpretation of precursors to PKP. Nature 240(5383):549–551

Cormier V (2000) D″ as a transition in the heterogeneity spectrum of the lowermost mantle. J Geophys Res 105(B7):16193–16205

Cormier V (2007) Texture of the uppermost inner core from forward- and back-scattered seismic waves. Earth Planet Sci Lett 258(3–4):442–453

Deschamps F, Cobden L, Tackley PJ (2012) The primitive nature of large low shear-wave velocity provinces. Earth Planet Sci Lett 349–350:198–208. doi:10.1016/j.epsl.2012.07.012

Doornbos D (1974) Seismic-wave scattering near caustics—observations of PKKP precursors. Nature 247(5440):352–353

Doornbos D (1978) Seismic-wave scattering by a rough core-mantle boundary. Geophys J R Astr Soc 53(3):643–662

Doornbos DJ, Husebye ES (1972) Array analysis of PKP phases and their precursors. Phys Earth Planet Inter 5:387–399. doi:10.1016/0031-9201(72)90110-0

Doornbos D, Vlaar N (1973) Regions of seismic-wave scattering in Earth's mantle and precursors to PKP. Nat Phys Sci 243(126):58–61
Dziewonski A, Anderson D (1981) Preliminary reference Earth model. Phys Earth Planet Inter 25(4):297–356
Earle P (2002) Origins of high-frequency scattered waves near PKKP from large aperture seismic array data. Bull Seism Soc Am 92(2):751–760
Earle PS, Rost S, Shearer PM, Thomas C (2011) Scattered P′P′ waves observed at short distances. Bull Seismol Soc Am 101(6):2843–2854. doi:10.1785/0120110157
Earle P, Shearer P (1997) Observations of PKKP precursors used to estimate small-scale topography on the core-mantle boundary. Science 277(5326):667–670
Earle P, Shearer P (1998) Observations of high-frequency scattered energy associated with the core phase PKKP. Geophys Res Lett 25(3):405–408
Earle P, Shearer P (2001) Distribution of fine-scale mantle heterogeneity from observations of P_{diff} coda. Bull Seism Soc Am 91(6):1875–1881
Frosch R, Green P (1966) Concept of a large aperture seismic array. Proc R Soc Lond 290(1422):368–388. doi:10.1098/rspa.1966.0056
Frost D, Rost S, Selby N, Stuart G (2013) Detection of a tall ridge at the core-mantle boundary from scattered PKP energy. Geophys J Int 195(1):558–574 (in print)
Fukao Y, Obayashi M, Nakakuki T (2009) Stagnant slab: a review. Ann Rev Earth Planet Sci 37:19–46. doi:10.1146/annurev.earth.36.031207.124224
Garnero E (2000) Heterogeneity of the lowermost mantle. Ann Rev Earth Planet Sci 28:509–537
Garnero E, McNamara A (2008) Structure and dynamics of Earth's lower mantle. Science 320(5876):626–628
Green P, Frosch R, Romney C (1965) Principles of an experimental large aperture seismic array (lasa). Proc IEEE 53(12):1821–1833
Gutenberg B, Richter C (1934) On seismic waves; I. Gerlands Beitr Geophysik 43:56–133
Haddon RAW, Cleary JR (1974) Evidence for scattering of seismic PKP waves near the mantle-core boundary. Phys Earth Planet Inter 8(3):211–234. doi:10.1016/0031-9201(74)90088-0
Haddon R, Husebye E, King D (1977) Origins of precursors to P′P′. Phys Earth Planet Inter 14(1):41–70
Hedlin MAH, Shearer PM, Earle PS (1997) Seismic evidence for small-scale heterogeneity throughout the Earth's mantle. Nature 387(6629):145–150. doi:10.1038/387145a0
Hedlin M, Shearer P (2000) An analysis of large-scale variations in small-scale mantle heterogeneity using global seismographic network recordings of precursors to PKP. J Geophys Res 105(B6):13655–13673
Hedlin M, Shearer P (2002) Probing mid-mantle heterogeneity using PKP coda waves. Phys Earth Planet Inter 130(3–4):195–208
Helffrich GR, Wood BJ (2001) The Earth's mantle. Nature 412(6846):501–507. doi:10.1038/35087500
Van der Hilst R, Engdahl E, Spakman W, Nolet G (1991) Tomographic imaging of subducted lithosphere below northwest Pacific island arcs. Nature 353(6339):37–43
Jeffreys SH, Bullen KE (1940) Seismological tables. Office of the British Association of Sciences
Kaneshima S (2009) Seismic scatterers at the shallowest lower mantle beneath subducted slabs. Earth Planet Sci Lett 286(1–2):304–315. doi:10.1016/j.epsl.2009.06.044
Kaneshima S, Helffrich G (1999) Dipping low-velocity layer in the mid-lower mantle: evidence for geochemical heterogeneity. Science 283(5409):1888–1891
Kaneshima S, Helffrich G (2003) Subparallel dipping heterogeneities in the mid-lower mantle. J Geophys Res 108(B5):2272
Kaneshima S, Helffrich G, Suetsugu D, Bina C, Inoue T, Wiens D, Jellinek M (2010) Small scale heterogeneity in the mid-lower mantle beneath the circum-Pacific area. Phys Earth Planet Inter 183(1–2):91–103. doi:10.1016/j.pepi.2010.03.011
Kennett B, Engdahl E (1991) Traveltimes for global earthquake location and phase identification. Geophys J Int 105(2):429–465
King D, Haddon R, Husebye E (1975) Precursors to PP. Phys Earth Planet Inter 10(2):103–127

King D, Husebye E, Haddon R (1976) Processing of seismic precursor data. Phys Earth Planet Inter 12(2–3):128–134

Kito T, Thomas C, Rietbrock A, Garnero E, Nippress SEJ, Heath AE (2008) Seismic evidence for a sharp lithospheric base persisting to the lowermost mantle beneath the Caribbean. Geophys J Int 174(3):1019–1028. doi:10.1111/j.1365-246X.2008.03880.x

Koper K, Franks J, Dombrovskaya M (2004) Evidence for small-scale heterogeneity in Earth's inner core from a global study of PKiKP coda waves. Earth Planet Sci Lett 228(3–4):227–241

Korn M (1988) P-wave coda analysis of short-period array data and the scattering and absorptive properties of the lithosphere. Geophys J Lond 93(3):437–449. doi:10.1111/j.1365-246X.1988.tb03871.x

Leyton F, Koper K (2007) Using PKiKP coda to determine inner core structure: 1. Synthesis of coda envelopes using single-scattering theories. J Geophys Res 112(B5):B05316

Li C, van der Hilst RD, Engdahl ER, Burdick S (2008) A new global model for P wave speed variations in Earth's mantle. Geochem Geophys Geosyst 9(5):Q05018. doi:10.1029/2007GC001806

Lithgow-Bertelloni C, Richards M (1998) The dynamics of Cenozoic and Mesozoic plate motions. Rev Geophys 36(1):27–78

Manchee E, Weichert D (1968) Epicentral uncertainties and detection probabilities from Yellowknife seismic array data. Bull Seism Soc Am 58(5):1359–1377

Mancinelli NJ, Shearer P (2013) Reconciling discrepancies among estimates of small-scale mantle heterogeneity from PKP precursors. Geophys J Int 195:1721–1729

Margerin L, Nolet G (2003) Multiple scattering of high-frequency seismic waves in the deep Earth: PKP precursor analysis and inversion for mantle granularity. J Geophys Res 108(B11):2514. doi:10.1029/2003JB002455

McNamara AK, Garnero EJ, Rost S (2010) Tracking deep mantle reservoirs with ultra-low velocity zones. Earth Planet Sci Lett 299(1–2):1–9. doi:10.1016/j.epsl.2010.07.042

McNamara A, Zhong S (2005) Thermochemical structures beneath Africa and the Pacific Ocean. Nature 437(7062):1136–1139

Olson P, Yuen D, Balsiger D (1984) Convective mixing and the fine-structure of mantle heterogeneity. Phys Earth Planet Inter 36:291–304

Poupinet G, Kennett BLN (2004) On the observation of high frequency PKiKP and its coda in Australia. Phys Earth Planet Inter 146(3–4):497–511

Ritsema J, Deuss A, van Heijst HJ, Woodhouse JH (2011) S40RTS: a degree-40 shear-velocity model for the mantle from new Rayleigh wave dispersion, teleseismic traveltime and normal-mode splitting function measurements. Geophys J Int 184(3):1223–1236. doi:10.1111/j.1365-246X.2010.04884.x

Rost S, Earle P (2010) Identifying regions of strong scattering at the core-mantle boundary from analysis of PKKP precursor energy. Earth Planet Sci Lett 297(3–4):616–626. doi:10.1016/j.epsl.2010.07.014

Rost S, Garnero E (2004) A study of the uppermost inner core from PKKP and P′P′ differential traveltimes. Geophys J Int 156(3):565–574

Rost S, Garnero E, Williams Q (2008) Seismic array detection of subducted oceanic crust in the lower mantle. J Geophys Res 113(B6):B06303. doi:10.1029/2007JB005263

Rost S, Thorne M (2010) Radial and lateral variations in mantle heterogeneity from scattered seismic waves (Invited). Abstract DI52A-08, 2010 Fall Meeting, AGU, San Francisco

Rost S, Thorne M, Garnero E (2006) Imaging global seismic phase arrivals by stacking array processed short-period data. Seism Res Lett 77(6):697–707

Sato H (1988) Temporal change in scattering and attenuation associated with the earthquake occurrence? A review of recent studies on coda waves. Pure Appl Geophys 126(2–4):465–497. doi:10.1007/BF00879007

Selby ND (2011) Improved teleseismic signal detection at small-aperture arrays. Bull Seismol Soc Amer 101(4):1563–1575. doi:10.1785/0120100253

Shearer P (1990) Seismic imaging of upper-mantle structure with new evidence for a 520-Km discontinuity. Nature 344(6262):121–126. doi:10.1038/344121a0

Shearer P, Earle P (2004) The global short-period wavefield modelled with a Monte-Carlo seismic phonon method. Geophys J Int 158(3):1103–1117
Shearer PM (2007) Deep Earth structure—seismic scattering in the deep Earth. Treatise on geophysics. Elsevier, Amsterdam, pp 695–729
Shearer PM, Earle PS (2008) Chapter 6—Observing and modeling elastic scattering in the deep Earth. In: Earth heterogeneity and scattering effects on seismic waves, vol 50. Elsevier, Amsterdam, pp 167–193
Simmons NA, Myers SC, Johannesson G, Matzel E (2012) LLNL-G3Dv3: global P wave tomography model for improved regional and teleseismic travel time prediction, J Geophys Res 117(B10). doi:10.1029/2012JB009525
Stixrude L, Lithgow-Bertelloni C (2012) Geophysics of chemical heterogeneity in the mantle. Ann Rev Earth Planet Sci 40(1):569–595. doi:10.1146/annurev.earth.36.031207.124244
Tan E, Gurnis M (2005) Metastable superplumes and mantle compressibility. Geophys Res Lett 32(20):L20307
Thomas C, Weber M, Wicks C, Scherbaum F (1999) Small scatterers in the lower mantle observed at German broadband arrays. J Geophys Res 104(B7):15073–15088
Tkalčić H, Flanagan M, Cormier V (2006) Observation of near-podal P′P′ precursors: evidence for back scattering from the 150–220 km zone in the Earth's upper mantle. Geophys Res Lett 33(3):L03305
Vanacore E, Niu F, Ma Y (2010) Large angle reflection from a dipping structure recorded as a PKIKP precursor: evidence for a low velocity zone at the core-mantle boundary beneath the Gulf of Mexico. Earth Planet Sci Lett 293(1–2):54–62. doi:10.1016/j.epsl.2010.02.018
Vidale J, Dodge D, Earle P (2000) Slow differential rotation of the Earth's inner core indicated by temporal changes in scattering. Nature 405(6785):445–448
Vidale J, Earle P (2000) Fine-scale heterogeneity in the Earth's inner core. Nature 404(6775):273–275
Weber M, Wicks C (1996) Reflections from a distant subduction zone. Geophys Res Lett 23(12):1453–1456
Weichert D, Whitham K (1969) Calibration of yellowknife seismic array with first zone explosions. Geophys J R Astr Soc 18(5):461–476
Wen L (2000) Intense seismic scattering near the Earth's core-mantle boundary beneath the Comoros hotspot. Geophys Res Lett 27(22):3627–3630
Widiyantoro S, Van der Hilst R (1997) Mantle structure beneath Indonesia inferred from high-resolution tomographic imaging. Geophys J Int 130(1):167–182. doi:10.1111/j.1365-246X.1997.tb00996.x
Woodhouse J, Dziewonski A (1984) Mapping the upper mantle—3-dimensional modeling of Earth structure by inversion of seismic waveforms. J Geophys Res 89(NB7):5953–5986
Wright C (1972) Array studies of seismic waves arriving between *P* and *PP* in distance range 90° to 115°. Bull Seismol Soc Amer 62(1):385–400